Barrier-Free Nucleation at Grain-Boundary Triple Junctions During Solid-State Phase Transformations

Huajing Song* and Jeffrey J. Hoyt†
Department of Materials Science and Engineering, McMaster University, Hamilton, L9H 4L7 Ontario, Canada
(Received 31 May 2016; published 30 November 2016)

Molecular dynamics simulations are used to provide strong evidence for barrier-free nucleation events in a heterogeneous solid-solid system. The barrier-free events are characterized by an absence of an incubation time and a growth rate of the emerging phase that is independent of the system size. Furthermore, an analysis of the size and shape of the critical nucleus using the Winterbottom construction indicates that no solution exists for these barrier-free cases. We propose that barrier-free nucleation, which will have a profound effect on phase transformation kinetics, may be a general phenomenon for any polycrystalline material.

DOI: 10.1103/PhysRevLett.117.238001

Nucleation is the most ubiquitous of all first-order phase transformations, but a complete theoretical understanding of the process remains elusive. According to the classical nucleation theory (CNT), the nucleation rate is extremely sensitive to material parameters that are difficult to independently measure, most notably the surface energy between nucleating and parent phase [1,2]. In the case of nucleation from a defect- and impurity-free bulk phase, which is homogeneous nucleation, careful experiments have been able to confirm the prediction of the CNT but only to within an accuracy of 1 or 2 orders of magnitude [3–6]. In recent years, stringent tests of the CNT have been provided by atomistic simulation where, instead of the nucleation rate, the size and work of formation of a critical nucleus are computed directly [5,7]. Although there exist several well-known extensions and corrections to the classical theory [8–10], the basic premise and predictions of the homogeneous CNT are generally accepted within the material science community.

In the case of heterogeneous nucleation, several surprising, and often unexplained, phenomena have been identified. As an example of so-called nonclassical nucleation [11], in an iron chloride magnetite precipitation experiment, Baumgartner *et al.* [12] indicated that the nucleation process can be conducted through pathways, involving different metastable clusters. In a study of polycrystalline colloidal systems, Peng *et al.* [13] have observed the grain-boundary nucleation of a second phase by a unique two-step process, where the grain boundary first undergoes a premelting event and subsequently the emerging phase forms by nucleation in the liquidlike film. In 2001, Offerman *et al.* [14] utilized x-ray diffraction from a synchrotron source to monitor grain-boundary nucleation kinetics of the body-centered cubic (bcc) ferrite (α) phase from the parent face-centered cubic (fcc) austenite (γ) phase in steels. The authors found that the experimental nucleation rates were at least 2 orders of magnitude faster than the predictions of the classical theory. A later paper [15] hypothesized that nucleation at grain corners or three-grain junctions may be characterized by a critical work of formation less than $1kT$ or by a completely barrier-free mechanism. Although barrier-free formation of phases at grain boundaries has been identified in some systems, most notably the formation of nonequilibrium complexions in ceramic materials [16], the case of steel represents an instance where an equilibrium phase forms at certain select grain-boundary locations in a relatively simple bcc-fcc system. More importantly, the suggestion of barrier-free nucleation in steels raises the possibility that the mechanism is quite general and may occur in many examples of solid-solid transformations in polycrystalline systems. Since the synchrotron experiments by Offerman *et al.* [14] were limited in resolution to nuclei > 2 μm, the critical nucleus size and shape could not be determined, and a direct confirmation of the barrier-free process could not be established. Therefore, the purpose of the present work is to present results from molecular dynamics simulations that strongly suggest a barrier-free nucleation event is possible in polycrystalline Fe. Although results from this study may be applicable to all polycrystalline materials, it should be noted that there are other examples of nucleation with extremely low energy barriers. For example, Rotter *et al.* [17] report a critical nucleus size of just one monomer during the polymerization of deoxygenated sickle hemoglobin, and Trujillo *et al.* [18] found that, during crystallization of polycaprolatone, carbon nanotubes are more potent heterogeneous nucleation sites than seed crystals of the stable phase.

Using molecular dynamics (MD) simulation, we systematically studied grain-boundary nucleation events that occur at the beginning of a solid-state transition in the isothermal condition. Six nanometer-scale pure Fe polycrystalline simulation cells were prepared according to the procedure outlined in previous publications [19,20] and in

Supplemental Material [21]. The xy dimension of the cells ranged from 40×40 to 100×100 nm^2, which accommodates 3–4γ-phase grains in the initial state. Full periodic boundary conditions were applied to avoid the influence of free surfaces. In order to reduce the number of atoms in the simulations, a quasi-2D geometry was chosen with the z dimension initially set to around 1.5 nm. When combined with periodic conditions, the small z thickness forces all the grain boundaries (GBs) and interfaces to be perpendicular to the xy plane; hence, the nucleus behaves as an infinitely long cylindrical disk within a single simulation cell. The interatomic potential used in all simulations was developed by Ackland *et al.* [30] (Supplemental Fig. S1), and the relevant properties, such as the free energy difference between the α and γ phases, have been computed previously [31]. Because of an absence of magnetic effects, the Fe potential cannot capture the correct phase equilibrium behavior of actual iron [32]. However, like most classical interatomic potentials, it reproduces quite well the energy of planar defects, and, as discussed below, barrier-free nucleation represents an interplay between a bulk driving force and interfacial energies, and we expect the results to be largely independent of the interatomic potential.

Consistent with the CNT, we found that nucleation was preferred at grain-boundary triple junctions in our simulations (no four-grain junctions were present in the quasi-2D geometry). In three of the total of six polycrystalline cells, we observed that the formation of a stable nucleus of the emerging α phase took place after an incubation time (lag time) of at least 0.5 ns (0.5–60 ns). However, for the remaining three starting configurations, we captured nuclei that formed at specific GB triple junctions with virtually no incubation time. In each of these cases, a nucleus, distinguished from atoms at the preexisting grain boundary, was detected within 0.02 ns, followed by a rapid growth of the new phase. The formation of the stable phase with no, or a very small, lag time is our first evidence of a barrier-free mechanism.

Figure 1 and Movie 1 show a typical example of the barrier-free nucleation process. The initial γ-phase polycrystalline system contains 409 600 atoms with a dimension of approximately $60 \times 60 \times 1.5$ nm^3. The simulation is run in a canonical (NVT) ensemble at 1000 K. Note that, with periodic boundary conditions, only four γ grains are present in the simulation cell [Fig. 1(a)]. In the figure, atoms are distinguished by their coordination number (CN) [19], and each image is first treated with an energy-minimization process [33] to remove the effects of thermal fluctuations. At $t = 0$ ns, virtually no α atoms are identified within the small observation window [the black box in Fig. 1(a)], indicating the nucleation is not activated by preexisting α clusters. At $t = 0.002$ ns [Fig. 1(b)], small numbers of α atoms appear around the center of the GB junction. Agglomerated α atoms are clearly detected from 0.005 ns, and then the nucleus grows rapidly along the GB

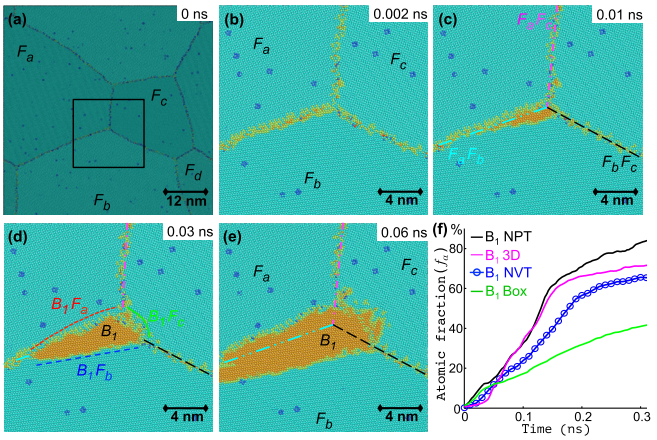

FIG. 1. Barrier-free nucleation at a triple GB junction. (a)–(e) Progress of nucleus B_1, atoms distinguished by CN, green (γ), orange (α), yellow (GB), and blue (defect). (f) bcc atomic ratio (f_α) vs time for nucleus B_1 for an NVT ensemble (blue line with circles), an NPT ensemble (black), in a fully 3D environment (magenta), and isolated in the dynamic region (green).

$F_a F_b$, as shown in Fig. 1(c) ($t = 0.01$ ns). The local bcc atomic fraction (f_α), which is the ratio of the bcc atoms to the total atoms within the observation window, is used to monitor the nucleation and growth process. As the blue line shown in Fig. 1(f) indicates, there is no significant plateau or inflections in the bcc evolution plot, which can be used to define the nucleation moment [13]. After 0.2 ns, the α phase almost completely fills the observation region, leading to a saturation of the f_α profile. To test the influence of stress and GB motion at a high temperature, the simulations were repeated in an isothermal-isobaric (NPT) ensemble to release the overall simulation cell pressure by adjusting the cell dimension every 1×10^{-4} ns. Also, at the simulation temperature of 1000 K, grain growth of the initial fcc structure takes place. To assess the effects of grain-boundary motion, as well as stress, additional simulations were performed where a dynamic box (where only the atoms within the box were allowed to move; see [20]) was positioned around the nucleus B_1, which restricted the GB motion. In the nucleation stage (0–0.02 ns), no significant changes were observed by varying the simulation settings above.

According to the CNT, the time lag is proportional to the interfacial area of the critical nucleus. In order to test this dependence, we have repeated the simulations described above but increased the thickness of the simulation box in the z direction. At the largest thickness studied $z = 9$ nm, the emerging nucleus no longer threads through the thin dimension and is entirely embedded within the interior of the cell. In other words, a fully 3D nucleation event is achieved. The curve labeled 3D in Fig. 1(f) shows the results of the 3D simulation, and it is clear that once again a very short or no incubation time exists. The fact that there is no dependence of early-stage nucleation kinetics on the

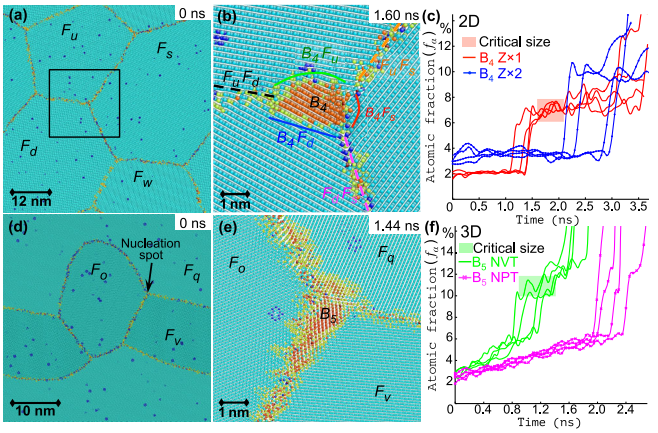

FIG. 2. Classical nucleation processes at triple GB junctions. (a) A quasi-2D system ($z = 1.2$ nm) of nucleus B_4. (b) Image of a critical nucleus. (c) bcc atomic ratio of nucleus B_4 ($Z \times 1$) and twice the z thickness ($z = 2.4$ nm) ($Z \times 2$). (d) and (e) show the nucleus B_5 that forms in a 3D system ($z = 9$ nm). (f) bcc atomic ratio of nucleus B_5 run in an NVT ensemble (green lines) and in an NPT ensemble (magenta lines).

system thickness is the second important indication that the process observed is barrier-free.

In contrast with the barrier-free phenomena, we also analyzed some nuclei forming at the GB junctions that showed classical behavior, two examples of which are shown in Fig. 2 (B_4 and B_5). Nucleus B_4 (Movie 2) was run in a quasi-2D system with dimension $65 \times 65 \times 1.4$ nm^3 (462 400 atoms). The simulation focused on a single GB junction; thus, it was restricted in a dynamic region [Fig. 2(a)] [20] to avoid the influence of barrier-free nucleation events at other three-grain junctions. Four separate MD runs were performed in NVT at 1000 K but with altered initial atom velocities. The results are plotted as red solid lines in Fig. 2(c). Note that the scales of the x and y axes in Fig. 2(c) are changed from the barrier-free case plotted in Fig. 1(f). After at least 1.0 ns of lag time, a rapid increase of the bcc atoms indicated an α particle is nucleating in the dynamic region [Fig. 2(c)]. The size of the critical α nucleus is estimated from the plateau region (shaded area) immediately after the rapid increase, because a critical nucleus is in unstable equilibrium and tends not to grow or shrink [13]. We also find that the nucleus sizes measured within these plateau regions are fairly steady (± 0.2 nm^2) from run to run. Figure 2(b) shows a snapshot of nucleus B_4 in the critical time region (1.60 ns), and the critical nucleus size was measured to be 2.9 nm^2 (Supplemental Fig. S3.2). According to the quasi-2D system geometry, the nucleus behaves as a thin cylindrical disk, whose nucleation energy should be related to the nucleus thickness. By repeating the simulation for different cell dimensions along the z periodic boundary, the nucleus volume and surface area are changed without influencing its cross-sectional area within the xy plane. The blue dotted line shown in Fig. 2(c) shows the results obtained for a z dimension, which is double that of the previous MD run (red curves). As expected from the CNT, the incubation period of nucleus B_4 is approximately doubled. Moreover, no nucleation was observed within 100 ns of simulation time for cell thicknesses greater than twice the original size.

Nucleus B_5 (Movie 3) was performed in a much thicker system ($45 \times 45 \times 9$ nm^3 and 1 382 400 atoms), which can be considered 3D. Unlike the 3D result shown in Fig. 1(f), there were no barrier-free nucleation events in this simulation cell, and all atoms were mobile during the simulation. A 4×4 nm^2 observation window was located on the first nucleation spot [Fig. 2(d)] to record the bcc atomic profile, which is shown in Fig. 2(f). A nucleation event was captured around 1.44 ns for the NVT ensemble with the cross-section image of the critical nucleus shown in Fig. 2(e). Since the new forming interfaces were not restricted to be perpendicular to the xy plane in 3D, the morphology of nucleus B_5 is much more complicated. In addition, as shown in Fig. 2(f), there is a significant difference in nucleation behavior for an NVT vs NPT simulation. Nevertheless, in either case there exists a nucleation lag time of at least 0.8 ns.

Our third indication that the process observed in the MD simulations is indeed barrier-free arises from an analysis from the CNT. The equilibrium shape of a nucleus for a given total area (volume in 3D) can be found using the Winterbottom construction [34,35] extended to the case of a three-grain junction [36,37]. The construction applied to a barrier-free nucleus B_1 is illustrated in Fig. 3(a). The blue curve represents the Wulff plot valid for homogeneous nucleation in the grain F_b. The anisotropic interfacial energies are determined by a procedure outlined in our previous publication [20] (also see Supplemental Fig. S2). The center of the blue Wulff plot is positioned at the intersection of the lines labeled $\sigma_{F_bF_c}$ and $\sigma_{F_aF_b}$. Also as shown, the lengths of these lines are proportional to the corresponding grain-boundary energies and are drawn perpendicular to the two boundaries F_bF_c and F_aF_b.

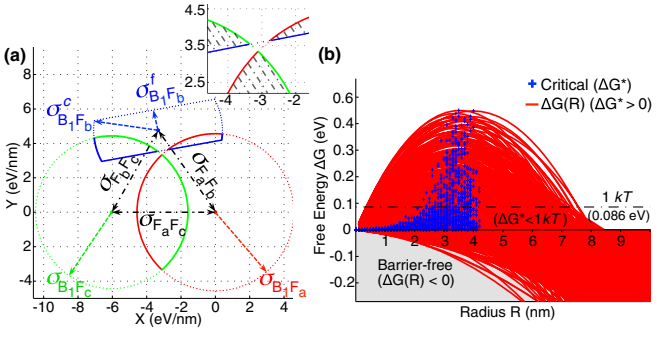

FIG. 3. (a) Winterbottom construction for nucleus B_1. A perfect wetting condition occurs at the GB junctions (inset). (b) Analysis of the uncertainty in the nucleation energies (see the text).

The red and green curves in Fig. 3(a) represent the Wulff plots describing the equilibrium shapes in the remaining two grains F_a and F_c, and their centers are found by a similar procedure as described above. According to the Winterbottom construction, the equilibrium nucleus shape is described by the region of overlap between the blue, red, and green curves. As clearly seen in the inset, for our best estimate for grain-boundary and interfacial energies (Supplemental Fig. S3.1), there is no overlap for the case of nucleus B_1, indicating that its formation requires no activation energy barrier. In computing the critical work of formation, we have neglected effects of Eshelby strain arising from the molar volume difference between the fcc and bcc phases. This assumption has been discussed and verified in several previous studies [38–41]. In addition, it should be noted that we have computed the excess GB and interfacial energies (i.e., at $T = 0$ K) and not the free energy. However, since these interfacial energies are known to decrease with an increasing temperature, including the actual σ values at the simulation temperature of $T = 1000$ K will lead to a decrease in the nucleation activation energy barrier, and the main conclusion, that is, an observation of a barrier-free event, is unchanged.

Although the results of Fig. 3(a) indicate a barrier-free nucleation process, there is considerable uncertainty in the computed values of all interface and grain-boundary energies. Therefore, to test if our conclusion is robust, we have performed the following error analysis. Once the shape of the critical nucleus is found from the Winterbottom construction, the work of formation (ΔG) vs some measure of the nucleus size can be plotted. For a representative size, we will use the radius of curvature, denoted R, of the surface with the greatest interfacial energy (B_1F_a in nucleus B_1). We then plot ΔG vs R for a total of 50 000 samples, where in each case the value of each interface and grain-boundary energy was selected randomly from a Gaussian distribution whose variance is equal to the uncertainty in each energy computation. The results of this Monte Carlo process are shown in Fig. 3(b). In 96% (gray) of the samples tested, there is no barrier to nucleation; that is, the work of formation is negative for all size nuclei. The small 4% of trials that resulted in an activation energy barrier are shown by the red curves in Fig. 3(b). The blue data points indicate the position of the critical size and critical nucleation energy (ΔG^*). For energies within the red band, although positive, most (3% of total samples) are quite small, i.e., less than $1kT$, which can be easily overcome by thermal fluctuations and can be considered barrier-free [15]. Less than 1% of the results fall into the classical nucleation regime, and the maximum nucleation barrier computed was $5kT$.

Similarly, the critical size and shape based on the Winterbottom construction were computed for classical nucleus B_4 (Supplemental Fig. S3.2), which formed from a quasi-2D structure with $z = 1.2$ nm. Figure 4(a) plots the free energy of nucleus B_4, with varying R. In Fig. 4(a), each individual contribution to the work of formation is plotted, the energy due to the α-γ interfacial energy is the top curve (blue), the GB energy, which is subtracted from the total, is shown in the dashed curve (pink), and the decrease in energy arising from the volume free energy difference between austenite and ferrite is given by the lowest (black) curve. The total work of formation is the solid green curve. As a result, the maximum ΔG value 3.6 eV is defined as the critical nucleation energy (ΔG^*), with the corresponding nucleation size 3.0 nm^2. Both the shape and critical size of nucleus B_4 predicted by the CNT are compatible with the observation from the MD simulations [Fig. 4(b)] (also see Supplemental Fig. S3.2). Again, an error analysis was performed [the red curve in Fig. 4(a)], and no test computations (out of 6000) revealed an entire downhill trajectory of ΔG. The possible nucleation energy barriers (blue +) are found to lie between 15 and $90kT$.

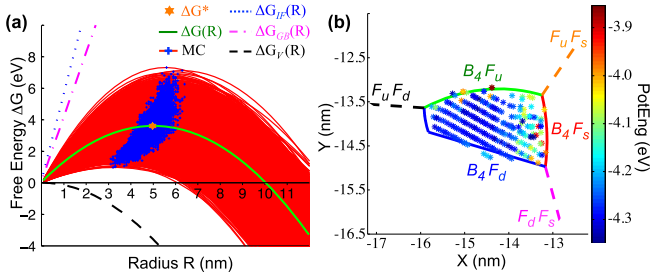

FIG. 4. (a) The free energy analysis of nucleus B_4, with a calculated nucleation energy barrier 3.6 eV and critical size 3.0 nm^2. (b) Comparison of the model results (solid and dashed lines) with MD observation (colored points, distinguished by potential energy). The critical size measured from the MD simulation was 2.9 ± 0.4 nm^2.

Recent experimental studies of solid-state phase transformations in steels have proposed that some nuclei with extremely low energy barriers [42,43] may generally form and their rate of formation cannot be described using the CNT framework. Since this barrier-free mechanism depends on the interplay between grain boundaries and new interfaces, we proposed the term structural barrier-free nucleation. In short, once the energy released from the vanished GBs completely compensates the energy cost to form new interfaces, the structural barrier-free nucleation occurs [21,44]. With an extremely small or nonexistent critical work of formation, the structural barrier-free phenomenon should occur rapidly at all undercoolings or even create prenucleating particles in a small range above the transition temperature. Meanwhile, the particular low energy interface structure characteristic of the barrier-free phenomenon should be ubiquitous in different heterophase polycrystalline material (e.g., hcp-fcc, diamond-wurtzite) or homophase grain boundaries (e.g., recrystallization [45]). Although the probability of a barrier-free nucleation event may be small, the growth rate of these nuclei is very

rapid, such that the overall transformation rate may depend to a large extent on the barrier-free mechanism, and including this contribution may explain the discrepancies between theory and experiment observed in previous studies.

In summary, MD simulations strongly suggest that, in pure Fe, the nucleation of the body-centered cubic phase at the grain boundaries of the face-centered cubic phase can occur in the absence of an activation energy barrier. The results of this study provide support for the previously proposed explanation for the long-standing disagreement between theory and experimental observations of the fcc-bcc phase transformation kinetics in steels, and *we propose that structural barrier-free nucleation may occur in any polycrystalline material*.

The authors acknowledge the support of a Natural Sciences and Engineering Research Council (NSERC, Canada) Strategic Project grant entitled "Simulation of complex microstructure path way for alloy design" and the computing resources of the Shared Hierarchical Academic Research Computing Network (Sharcnet) of Ontario. We gratefully acknowledge numerous helpful discussions with Dr. Gary Purdy and Dr. Hatem S. Zurob. H. S. acknowledges financial support from a NSERC postgraduate doctoral scholarship (NSERC PGS-D).

*Present address: Division of Materials Sciences and Engineering, Ames Laboratory, Ames, IA 50011, USA
songhw@ameslab.gov
†hoytj@mcmaster.ca

[1] D. Kashchiev, *Nucleation: Basic Theory with Applications* (Butterworth-Heinemann, London, 2000).
[2] K. F. Kelton and A. L. Greer, Phys. Rev. B **38**, 10089 (1988).
[3] R. Heady and J. Cahn, J. Chem. Phys. **58**, 896 (1973).
[4] E. D. Siebert and C. M. Knobler, Phys. Rev. Lett. **52**, 1133 (1984).
[5] J. Bokeloh, G. Wilde, R. Rozas, R. Benjamin, and J. Horbach, Eur. Phys. J. Spec. Top. **223**, 511 (2014).
[6] F. LeGoues and H. Aaronson, Acta Metall. **32**, 1855 (1984).
[7] S. Auer and D. Frenkel, Nature (London) **413**, 711 (2001).
[8] J. S. Langer and A. J. Schwartz, Phys. Rev. A **21**, 948 (1980).
[9] Q. Hu *et al.*, Faraday Discuss. **159**, 509 (2012).
[10] L. Granasy, T. Pusztai, D. Saylor, and J. A. Warren, Phys. Rev. Lett. **98**, 035703 (2007).
[11] W. Habraken *et al.*, Nat. Commun. **4**, 1507 (2013).
[12] J. Baumgartner, A. Dey, P. H. H. Bomans, C. Le Coadou, P. Fratzl, N. A. J. M. Sommerdijk, and D. Faivre, Nat. Mater. **12**, 310 (2013).
[13] Y. Peng, F. Wang, Z. Wang, A. M. Alsayed, Z. Zhang, A. G. Yodh, and Y. Han, Nat. Mater. **14**, 101 (2015).
[14] S. E. Offerman, N. H. van Dijk, J. Sietsma, S. Grigull, E. M. Lauridsen, L. Margulies, H. F. Poulsen, M. T. Rekveldt, and S. van der Zwaag, Science **298**, 1003 (2002).
[15] N. van Dijk, S. Offerman, J. Sietsma, and S. van der Zwaag, Acta Mater. **55**, 4489 (2007).
[16] D. R. Clarke, Annu. Rev. Mater. Sci. **17**, 57 (1987).
[17] M. Rotter, S. Kwong, R. Briehl, and F. Ferrone, Biophys. J. **89**, 2677 (2005).
[18] M. Trujillo, M. Arnal, A. Muller, M. Mujica, C. Urbina de Navarro, B. Ruelle, and P. Dubois, Polymer **53**, 832 (2012).
[19] H. Song and J. J. Hoyt, Model. Simul. Mater. Sci. Eng. **23**, 085012 (2015).
[20] H. Song and J. J. Hoyt, Comput. Mater. Sci. **117**, 151 (2016).
[21] See Supplemental Material at http://link.aps.org/supplemental/10.1103/PhysRevLett.117.238001 for details of the MD simulation procedures and the Winterbottom analysis, which includes Refs. [22–29].
[22] J. J. Hoyt, *Phase Transformations* (Cambridge University Press, Cambridge, England, 2000), Chap. 8.
[23] J. Lee and H. Aaronson, Acta Metall. **23**, 809 (1975).
[24] J. Lee and H. Aaronson, *Lectures on the Theory of Phase Transformations*, 2nd ed. (Wiley-TMS, New York, 1999), pp. 165–229.
[25] E. M. Lopasso, M. Caro, A. Caro, and P. Turchi, Phys. Rev. B **68**, 214205 (2003).
[26] M. Mendelev, M. Asta, M. Rahman, and J. J. Hoyt, Philos. Mag. **89**, 3269 (2009).
[27] H. Song, Ph. D thesis, Department of Materials Science and Engineering, McMaster University, 2016.
[28] H. Song and J. J. Hoyt, Acta Mater. **61**, 1189 (2013).
[29] W. Winterbottom, Acta Metall. **15**, 303 (1967).
[30] G. Ackland, D. Bacon, A. Calder, and T. Harry, Philos. Mag. A **75**, 713 (1997).
[31] H. Song and J. J. Hoyt, Acta Mater. **60**, 4328 (2012).
[32] A. Caro, P. Turchi, M. Caro, and E. Lopasso, J. Nucl. Mater. **336**, 233 (2005).
[33] LAMMPS, Sandia National Laboratories (http://lammps.sandia.gov).
[34] R. Zucker, D. Chatain, U. Dahmen, S. Hagege, and W. Carter, J. Mater. Sci. **47**, 8290 (2012).
[35] J. Lee and H. Aaronson, Acta Metall. **23**, 799 (1975).
[36] J. Lee and H. Aaronson, Scr. Metall. **8**, 1451 (1974).
[37] M. Fewell, Ph. D thesis, Defence Science and Technology Organisation, 2006.
[38] H. Aaronson, M. Hall, D. Barnett, and K. Kinsman, Scr. Metall. **9**, 705 (1975).
[39] M. Hall, H. Aaronson, and K. Kinsma, Surf. Sci. **31**, 257 (1972).
[40] J. Eshelby, Proc. R. Soc. A **241**, 376 (1957).
[41] W. F. Lange, M. Enomoto, and H. I. Aaronson, Metall. Trans. A **19**, 427 (1988).
[42] M. Enomoto and J. B. Yang, Metall. Trans. A **39**, 994 (2008).
[43] V. I. Savran, S. E. Offerman, and J. Sietsma, Metall. Trans. A **41**, 583 (2010).
[44] This mechanism corresponds to region C according to the scheme outlined by van Dijk *et al.* [15].
[45] B. Lin, Y. Jin, C. Hefferan, S. Li, J. Lind, R. Suter, M. Bernacki, N. Bozzolo, A. Rollett, and G. Rohrer, Acta Mater. **99**, 63 (2015).